Electrified Postsunrise Ionospheric Perturbations at Millstone Hill

Citation: Zhang, Shun#Rong, Erickson, Philip J., Gasque, L. C., Aa, Ercha, Rideout, William et al. 2021. "Electrified Postsunrise Ionospheric Perturbations at Millstone Hill." Geophysical Research Letters, 48 (18).

As Published: http://dx.doi.org/10.1029/2021gl095151

Publisher: American Geophysical Union (AGU)

Persistent URL: https://hdl.handle.net/1721.1/140567

Version: Author's final manuscript: final author's manuscript post peer review, without publisher's formatting or copy editing

Electrified postsunrise ionospheric perturbations at Millstone Hill

Shun-Rong Zhang[1], Philip J. Erickson[1], L. C. Gasque[1,2], Ercha Aa[1], William Rideout[1], Juha Vierinen[3], Larisa P. Goncharenko [1], Anthea J. Coster[1]

[1]Haystack Observatory, Massachusetts Institute of Technology
[2]Space Sciences Laboratory, University of California at Berkeley
[3]University of Tromsø, Tromsø, Norway

Key Points:

- Postsunrise midlatitude periodic traveling ionospheric disturbances occur, propagating eastward with downward phase progression
- Periodic polarization electric fields in meridional direction were embedded in traveling ionospheric disturbances, large in the morning
- The electrified ionospheric waves are possibly due to gravity wave wind-induced F-region dynamo effects

Corresponding author: Shun-Rong Zhang, shunrong@mit.edu

Abstract

We provide evidence that midlatitude postsunrise traveling ionospheric disturbances (TIDs) are comprised of electrified waves with an eastward propagation component. The post-sunrise gravity wave (GW) wind-induced dynamo action effectively generated periodic meridional polarization electric fields (PEFs), facilitating TID zonal propagation in a similar fashion as GW-driven neutral perturbations. A combination of near-simultaneous eastward and upward observations using the Millstone Hill incoherent scatter radar along with 2-dimensional total electron content maps allowed resolution of TID vertical and horizontal propagation as well as zonal ion drifts V_{east} (meridional PEFs). In multiple observations, V_{east} oscillated in the early morning during periods when TIDs exhibited downward phase progression, 30-60 min period, ~140 m/s eastward speed, and 70 km vertical wavelength. Inside these TIDs, multiple flow vortexes occurred in a vertical-zonal plane spanning the ionospheric topside and bottomside. Subsequently, PEFs weakened after a few hours as TID horizontal wavefronts rotated clockwise.

Plain Language Summary

The solar terminator (ST) provides a repeatable, regulated forcing to the upper atmosphere, exciting thermospheric and ionospheric waves. These waves have zonal propagation components due to the terminator's orientation. Nominally, traveling ionospheric disturbances (TIDs) are considered a manifestation of dynamics produced by propagating thermospheric waves such as gravity waves (GWs). However, GW zonal propagation would be expected to be greatly attenuated in the F region since ions cannot easily move zonally across the meridionally oriented magnetic field. This study provides evidence that midlatitude postsunrise TIDs are electrified waves, due to meridional polarization electric fields (PEFs) embedded in the TIDs. We also identified plasma flow vortexes in a vertical-zonal plane. Although observed TIDs possess some general GW characteristics, their manifestation is more complex. Particularly, GW wind-induced dynamo action can generate oscillating PEFs and facilitate TID zonal propagation. Our results imply the importance of electrodynamics in understanding the dynamics of ST-time ionospheric waves. Observations used the Millstone Hill incoherent scatter radar to measure TIDs and their zonal and vertical propagation, as well as F-region plasma zonal drifts (driven by PEFs) during TID/GW passage. GNSS data were used to provide 2D TID wave characteristics.

1 Introduction

As the solar terminator (ST) sweeps through the Earth's atmosphere, sharp gradients in solar illumination across ST and their movement (with both supersonic and subsonic components) can induce disturbances in the atmosphere and ionosphere (Somsikov, 2011). Theoretical calculations and observational studies have focused on ST induced waves, with an emphasis on atmospheric gravity waves (GWs) associated with ST occurring in different layers of the atmosphere (Beer, 1973; Somsikov & Trotskii, 1975; Beer, 1978; Vasylyev & Sergeev, 1999; Forbes et al., 2008; H. Liu et al., 2009; Miyoshi et al., 2009; Hedlin et al., 2018). In particular, the lower atmosphere source regions of ST induced GWs are thought to be the ozone layers which efficiently absorb UV heating, as first pointed out by Chimonas and Hines (1970) and Chimonas (1970) in solar eclipse studies.

However, because of the charged nature of the ionosphere and the presence of a strong background magnetic field, ionospheric response to ST forcing is more complicated and takes a variety of forms. First, under strong ion-neutral coupling, ionospheric density can be perturbed by ST-induced GWs, taking the form of traveling ionospheric disturbances (TIDs), as reported previously (e.g. Galushko et al., 1998; Afraimovich et al., 2010; Song et al., 2013; Nygrn et al., 2015). Support for the TID-ST connection is reinforced by separate studies of TID excitation near ST by a solar flare, causing sharply enhanced solar irradiation (S.-R. Zhang et al., 2019), and by solar eclipses with sharply reduced solar irradiation (J. Y. Liu et al., 2011; S.-R. Zhang, Erickson, Goncharenko, et al., 2017; Eisenbeis et al., 2019). Further complexity in ionospheric response dynamics is evident in numerous sunrise ionospheric phenomena (Rishbeth & Setty, 1961; Evans, 1968; Rishbeth et al., 1995), electrodynamic effects (Kelley et al., 2014; R. Zhang et al., 2015; Chen et al., 2020; Zhu et al., 2017), plasma instability intensification / excitation at equatorial latitudes, and magnetosonic wave excitation at high altitudes along magnetic field lines (Afraimovich et al., 2009; Huba et al., 2000).

ST-induced GWs are likely to have propagation components in both the zonal direction, perpendicular to the meridionally-oriented ST, and the vertical direction. In the ionosphere, however, the F-region plasma experiences significant resistance to zonal motion due to the largely meridional magnetic field at mid- and low latitudes. Consequently, GW (and therefore TID) zonal propagation should be substantially suppressed (C. H. Liu

& Yeh, 1969) because of the ion-neutral coupling via ion drag or "ohmic loss" damping effect (e.g. Hines & Hooke, 1970; Medvedev et al., 2017). Significant TID zonal motions at sunrise therefore require an additional mechanism involving the generation of meridional polarization electric fields (PEFs) which subsequently influence plasma electrodynamics in the F region. Under this scenario, ST associated TIDs are electrified, although GWs remain fundamental in initiating such PEFs and driving plasma disturbance propagation along with GWs. Along these lines, previous studies have indicated that the GW wind dynamo action can induce PEFs, particularly when the wavefronts are aligned in the meridional/magnetic field direction (e.g. Tsunoda, 2010; Krall et al., 2013; Huba et al., 2015; Chou et al., 2018; Hysell et al., 2018). In another example, Varney et al. (2009) presented Jicamarca incoherent scatter radar (ISR) observations of nighttime electric fields generated by GWs whose propagation vectors were nearly perpendicular to the magnetic meridian.

The present study analyzes post-sunrise zonal propagation of TIDs and the associated electrodynamics across ST and in later daytime hours. We provide the first evidence of midlatitude morning-time periodic PEFs likely induced by terminator-associated GWs. These results imply the importance of electrodynamics in understanding the ST-time ionospheric waves. This study is based on MH ISR observations in the mornings in June 2018 – September 2020.GNSS TEC are also used to provide 2-D visualization of ionospheric wavefronts.

2 Observations

A series of sunrise ISR experiments at Millstone Hill (MH) (42.6°N, 288.5°E) were conducted to detect ionospheric disturbances and their zonal propagation across sunrise and throughout sunlit hours. These were on (year–month–day) 2018-09-04, 2018-10-19, 2018-10-22, 2018-11-09, 2018-12-12, 2019-01-17, 2020-01-29, and 2020-02-19. During each experiment, both the conventional ion-acoustic resonance "ion-line" and the Langmuir resonance "plasma-line" data were obtained. The latter yields 90-second time resolution and $<\sim 0.1\%$ uncertainty in plasma frequency, highly appropriate for ionospheric wave studies (Djuth et al., 2004). Plasma-line echoes have been regularly observed at MH since 2016, with analysis for plasma density determination using a similar procedure as in Vierinen et al. (2016). Currently, the strongest plasma-line echo, corresponding to the F2 electron density peak during sunlit hours, is continuously recorded. The study of S.-R. Zhang et al. (2019) gave an example of F2- and F1-peak plasma-line observations during a solar flare.

The experiments reported here utilized the zenith and steerable (MISA) antennas alternatively, each with 90 second dwell, for two near-simultaneous measurements resolving ionospheric waves with periodicities as short as minutes. The MISA antenna was pointed eastward at $\sim 67°$ elevation. Thus, the ionospheric volume at 210 km [300 km] altitude, which was close to the F2-peak height for most of these deep solar minimum experiments, was separated zonally by 89 km [127 km] between the MISA and zenith beams. Assuming a zonal propagation speed between 100-500 m/s, the lag time for wave perturbations to travel between the two F region volumes at 89 km [127 km] separation would be approximately 15-3 min [21-4 min]. The radar also measured the regular "ion line" to yield standard plasma state parameters as a function of altitude including electron density (Ne) and line-of-sight (LOS) ion drift. Waveforms used interleaved long-pulse (LP; ~36 km effective range resolution) and alternating code (AC; $\sim$ 4.5 km effective range resolution) schemes. As the 90-second integration time was too short for good quality ion-line data, post-integration in each bin was further performed with sliding windows in ±10-min time and ±10 km (AC) or 20 km (SP) range to improve statistical uncertainty of measured Ne and ion drifts, particularly the zonal ion drift V_{east} (positive east). Typically there were $\sim$ 25 data points in each smoothing bin. By combining the LOS data from both antennas, V_{east} was straightforwardly determined. The calculated V_{east} uncertainty is dominated by measured LOS uncertainty, which is roughly estimated at 20-40 m/s in a bin (c.f. Figure 2d,e), becoming larger below 200 km altitude at night and in early morning hours. The measured V_{east} is in the geographic east. With 12.7° magnetic declination D and 69° dip I in the F region, the field-aligned drift contributes to V_{east} through a very small projection factor of 0.078 (=$\sin D \cos I$),

GNSS TEC observations were also used to provide 2-dimensional context of TIDs in the MH vicinity. A global GNSS database from 6000+ receivers was utilized to yield ionospheric disturbances in differential TEC (dTEC) after de-trending the background TEC variations determined by a low-pass filter (Savitzky & Golay, 1964). A 30-min sliding window and a linear basis function for the filter were used, as described in (S.-R. Zhang, Erickson, Goncharenko, et al., 2017; S.-R. Zhang et al., 2019).

We use observations on 2018-09-04 and 2020-01-29 as representative of characteristic TID and V_{east} variations occurring across all the sunrise experiments. We note that these intervals were not completely quiet geomagnetically. On 2018-09-04, the AE index reached 500 nT for an hour at ∼06 UT, and 2020-01-29 had a similar AE maximum of ∼500 nT briefly at 12 UT. However, although these geomagnetic activities caused some equatorward small-amplitude, large-scale TIDs (LSTIDs) over MH, wavefronts were broad in latitudinal span and zonally elongated, and therefore were separable from post-sunrise medium-scale TIDs (MSTIDs) which are the prime type of TIDs investigated here.

3 Results

On 2018-09-04, plasma-line F2 peak density Nmax measured on both radar antennas exhibited clear oscillations throughout sunlit hours (Figure 1a). Even though the local sunrise above zenith was 1 min later than that to the east where the MISA beam intersected the F-region (and thus the ionization build-up above zenith occurred slightly later), zenith TID data had earlier disturbance phases than those in MISA data. These phase lags lasted for ∼4 hours (the green bar in Figure 1a), and cross-correlation analysis in Figure 1b quantified the lag at ∼11 min, implying an eastward propagation at 135 m/s at 210 km altitude. Since observed TIDs had predominantly a ∼55 min period, the zonal wavelength was estimated at ∼445 km.

GNSS dTEC provided 2D context for TIDs resolved by the radar. Clear zonal propagation was observed in the dTEC keogram, especially near the Atlantic coast (Figure 1d). On average, the zonal phase speed was ∼ 148 m/s (assuming 210 km height), a value very close to the plasma-line result. The GNSS zonal wavelength was ∼425 km, also very close to the plasma-line result. Near the terminator, V_{east}, Vo and Ne showed large fluctuations, some of the TID fronts seemed elongated meridionally (Figure 1e,f), and in later times (after 1400 UT) away from the terminator, the fronts were rotated clockwise and had fairly large zonal components (Figure 1e,g).

Beyond 190–220 km altitude where the F region peak density occurred, Ne throughout the F-region oscillated as well (Figure 2a). Ne fluctuations (dNe) as a percentage deviation (from the 2-hour running average) showed clear downward phase progression, a typical characteristic for GW-induced fluctuations. Wave phase did not change very much above the F2 peak. TID amplitude was 15%, larger in the early morning, and vis-

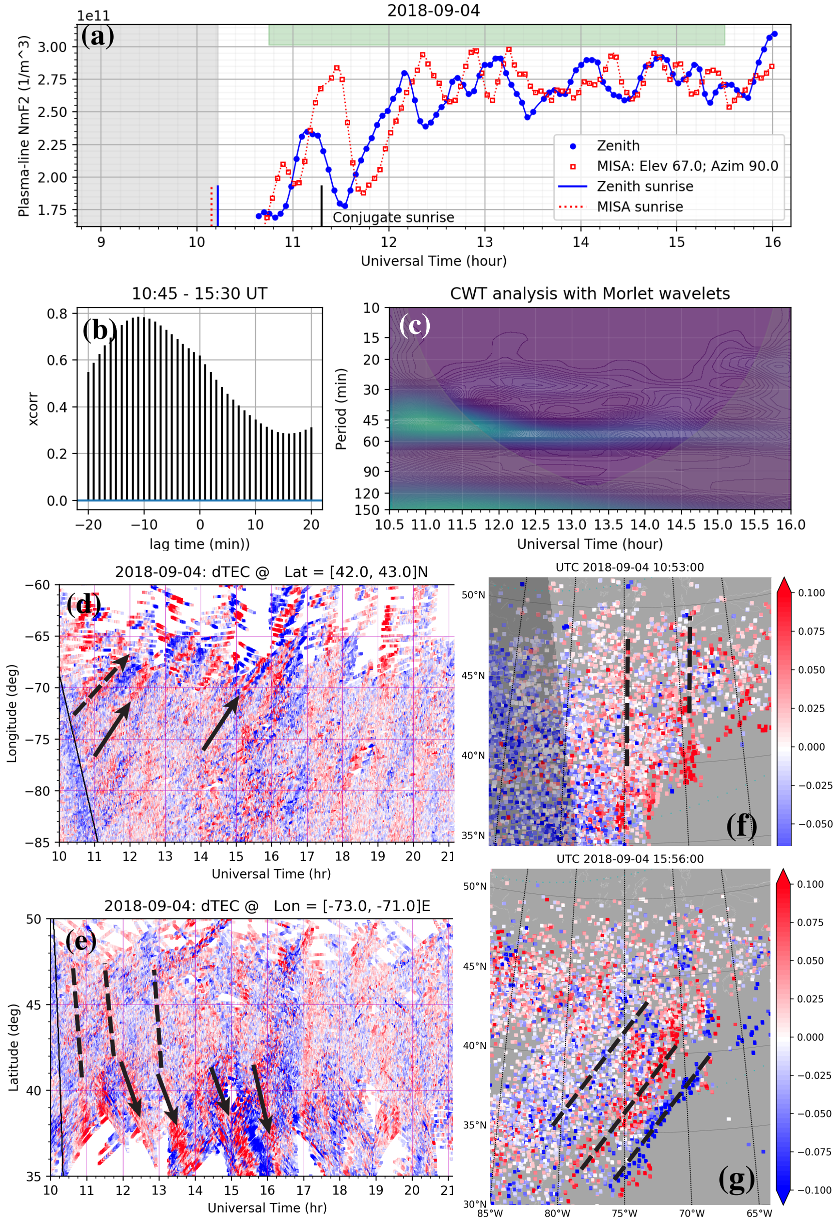

Figure 1. 2018-09-04 TIDs observed with ISR (a-c) and GNSS (d-g): Plasma-line Nmax from zenith and MISA antennas (a); their cross-correlation coefficient as a function of MISA-to-Zenith lag time (b); periodicity of zenith data derived using Morlet wavelets with shaded cones of influences (c.f. Mallat (1999)) (c); GNSS dTEC keograms as a function of UT and longitude for MH latitudes (42-43°N) (d), as a function of UT and latitude for MH longitudes (-73 to -71°E) (e); some example TIDs, with partial wavefronts meridionally elongated at 10:35 UT (f); and larger wavefronts clockwise-rotated at 15:56 UT (g). GNSS plots share the same color bar. Black solid lines in (d-e) are sunrise terminators.

ible as low as 125 km altitude. This amplitude is typical at MH (e.g. Galushko et al., 1998; Panasenko et al., 2018) but seems larger than several other observations (e.g. Kirchengast et al., 1996) and smaller than those during geomagnetic storms (e.g. S.-R. Zhang, Erickson, Zhang, et al., 2017). The vertical wavelength was ~70 km and vertical phase speed was ~ 20 m/s.

Vertical ion drift Vo above 250 km (above the F2 peak) had a prominent sign change from downward to upward around sunrise, followed by oscillations with 50-60 min periodicities and decreasing amplitudes over time (Figure 2b). Zonal speed V_{east} was estimated at ±80 m/s (2 mV/m equivalent electric field). Obvious quasi-periodic oscillations (but more negative, or westward) occurred before 13:30 UT (08:45 LT) in the early morning hours, with slower but more steady eastward speeds at later times (pre-noon) (Figure 2c,d). Early morning oscillations in V_{east} appeared strongly correlated to Ne and Vo fluctuations, both of which had large amplitudes: pre-sunrise downward Vo correlated to eastward V_{east} (in the topside), and post-sunrise upward Vo correlated to westward V_{east} (Figure 2c,d). Observations showed another very remarkable feature: V_{east} in the topside and bottomside ionosphere, measured using totally different radar pulse schemes (AC below, LP above), was highly correlated but with opposite directions during the morning hours (Figure 2d,e).

A second experiment example on 2020-01-29 showed similar ST-time oscillations as seen in Figure 3. During early morning hours (prior to 16 UT, or ~11 SLT), ~145 m/s east propagation in both radar and GNSS data was observed (Figure 3a,c). The detected zonal propagation was consistently <200 m/s, lower than reported in Galushko et al. (1998); Song et al. (2013). Later, the wavefronts rotated clockwise with a larger equatorward wave vector (Figure 3a,e). The rotation could be related to background thermospheric changes or arrival of other disturbances (e.g., minor magnetic disturbances).

4 Discussion

The ST-time observation series can be typically represented by the 2018-09-04 experiment summary: (1) TIDs following sunrise had their eastward propagation at 140 m/s phase speed and ~420 km wavelength, and downward phase progression with 70 km vertical wavelength; (2) V_{east} observations in the early morning provided evidence of oscillating polarization electric fields (PEFs) that accompanied dNe and Vo oscillations.

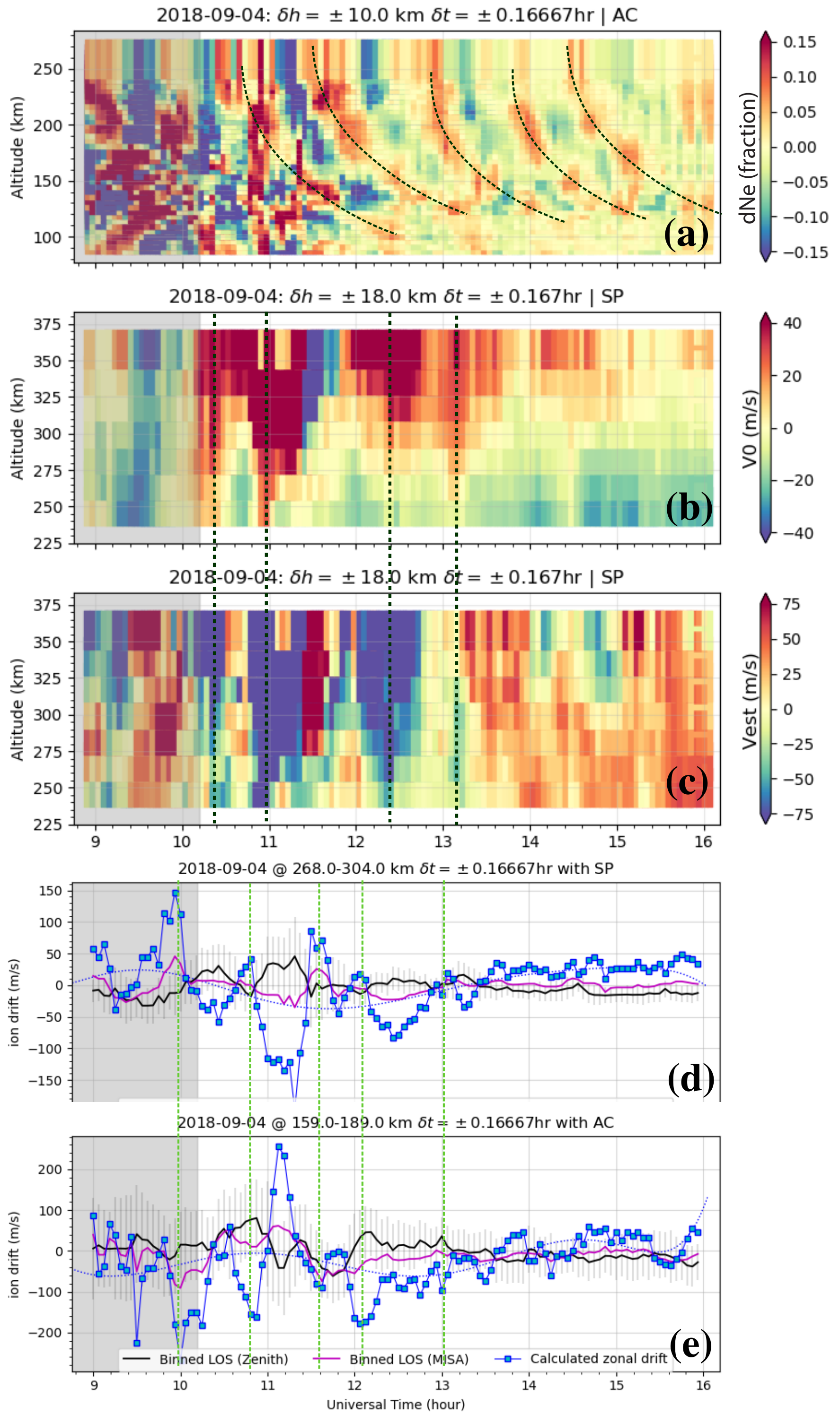

Figure 2. Radar "ion-line" Ne between 100-250 km on 2018-09-04 as percentage deviation (dNe) from the 2-hour running average using AC pulse scheme (a), vertical ion drift Vo between 250-375 km using LP scheme (b), and calculated eastward ion drift V_{east} between 250-375 km (c). Line plots show LOS medians (with error bars being bin standard deviation for zenith LOS, Vo) and V_{east} for a topside altitude bin (d), and bottomside bin (e).

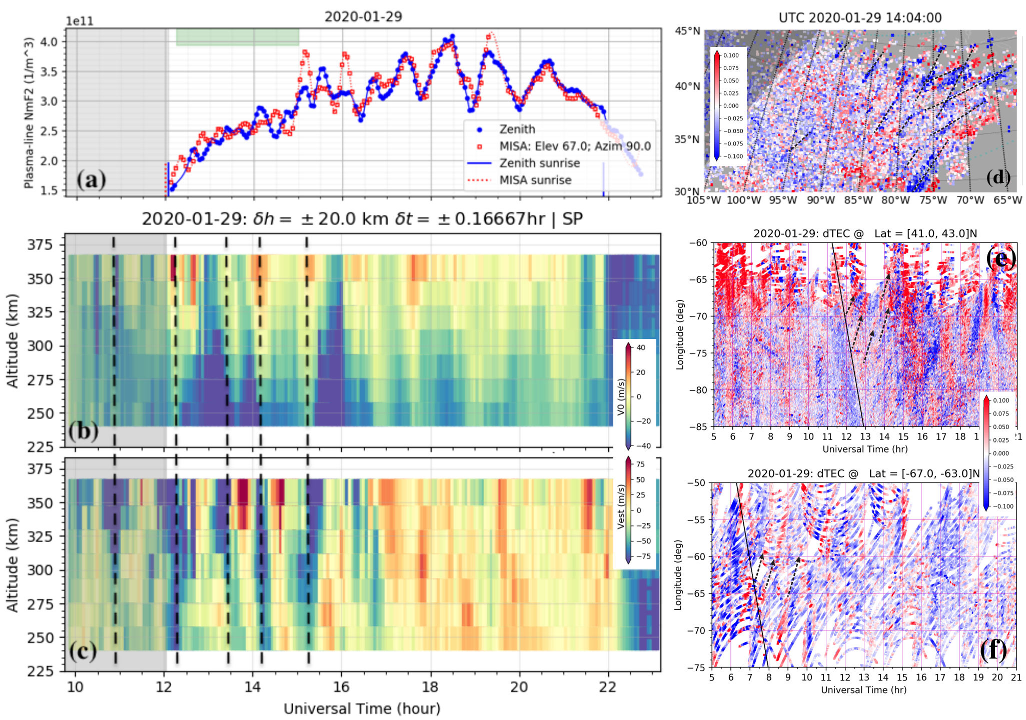

Figure 3. 2020-01-29 ISR and GNSS observations: plasma-line Nmax on zenith and MISA antennas (a); vertical drift (b) and eastward drift V_{east} (c) both in the topside above 250 km; GNSS dTEC map at 14:04 UT (d), longitudinal dTEC keograms at MH (e) and its conjugate Palmer (f) latitudes, respectively. Solid lines in (e-f) are sunrise terminators.

4.1 Wave periodicity and wavefront orientation

Assuming the ST-time TIDs were GW manifestations, a 55-min wave periodicity on 2018-09-04 implies the GW propagation elevation $\gamma = \arctan\sqrt{(\omega_B^2/\omega^2 - 1)} \sim 74$–80° with ω and ω_B being TID angular frequency and Brunt-Väisälä frequency (assuming 10-15 min periods at 200 km). The 2020-01-29 observation (Figure 3) had a 30-45 min periodicity in the early morning (marked by a green bar in Figure 3a), and thus they would have $\gamma \sim 60$-77° with more appreciable horizontal wave number and would be more likely ST wave candidates than those reported previously with 90-120 min periods (Galushko et al., 1998). Across all ST-time experiments (not presented here), we observed wave periods normally between 30-60 min, considerably longer than 10-20 min reported in a GNSS statistics work by Afraimovich et al. (2010). It should be noted these observed periods are not intrinsic periods thus the above comparisons are meaningful only when the background winds are comparable, which might be the case under these sunrise conditions.

In aggregate, TID eastward propagation was clearly preferable in the morning. This time-frame is consistent with Afraimovich et al. (2010) who reported the occurrence of TIDs within 3 hours of ST passage. It should be noted though that zonal propagation in all experiments was **eastward**, similar to Galushko et al. (1998), but **opposite to** the Song et al. (2013) statistics, which indicated overwhelming westward propagation of LSTIDs near sunrise ST throughout the year in the Chinese longitude sector. The reason for this discrepancy remains for future study.

4.2 TID electrodynamics

The 2020-01-29 case was also characterized by quasi-periodic Vo and V_{east} fluctuations (Figure 3b,c) which provided a consistent physical picture as in the 2018-09-04 case. Meridional PEFs induced V_{east} in the F region had larger amplitudes in the early morning hours, and were strongly correlated to Vo and Nmax fluctuations.

Although our main focus is not to determine whether ST had ultimately caused these GWs with an apparent zonal propagation, overall wave properties of observed TIDs in both vertical and zonal directions are reasonably consistent with general GW dispersion theories (e.g. Vadas, 2007). However, the ionospheric plasma exhibited unique electrodynamic behavior in the form of TID zonal propagation. In particular, distinct V_{east}

oscillations, occurring with large TID morning oscillations in dNe and Vo, imply that PEFs were embedded in TIDs and possibly generated by GWs, as elaborated below.

Neutral wind (especially zonal wind) dynamo effects across ST are known in particular for generating the prominent evening pre-reversal enhancement in vertical drift Vo at low latitudes (e.g. Farley et al., 1986; Haerendel & Eccles, 1992; Eccles et al., 2015; Heelis et al., 2012). These effects may also contribute to a similar morning drift enhancement (Kelley et al., 2014; R. Zhang et al., 2015; Chen et al., 2020). Our observations provided a similar Vo variation pattern: downward before and upward after sunrise. Figure 4a show schematic diagrams of zonal wind dynamo effects in the F-region. Eastward winds $\mathbf{U}$ drive Pedersen currents $\mathbf{J}_p$ in $\mathbf{U} \times \mathbf{B}$ (meridional) direction. These currents generate F-region meridional PEFs $\mathbf{E}_p$ which cannot be short-circuited by E-region currents, since conductivities are discontinuous across the ST. Therefore PEFs $\mathbf{E}_p$ driven by zonal winds will drive V_{east} in the same direction as zonal winds (Rishbeth, 1971). The eastward zonal-wind dynamo mechanism is sufficient to explain eastward V_{east} on the nightside near ST (Figures 2c and 3c), even without GWs. It should be noted that midlatitude zonal winds change their direction from eastward to westward around the morning ST due to the zonal pressure gradient buildup in the thermosphere, and therefore V_{east} is generally more westward in the morning (10-13 UT for 2018-09-04 and 12-17 UT for 2020-01-29). It is more eastward afterwards, possibly due to the E-region dynamo during the day (Heelis, 2004).

Even though zonal oscillations can be driven electrodynamically, we further argue that GWs remain necessary conditions for post-sunrise V_{east} oscillations. Figures 4b,c depict morning GW zonal wind dynamo effect. Again, F-region meridional PEFs are directed opposite to the direction of zonal-wind driven Pedersen currents, and V_{east} and $\mathbf{U}$ are in the same direction. The PEFs may be sustained before they are completely short-circuited by E-region currents or currents in the conjugate hemisphere. The post-sunrise electron density build-up progression in the E-region is important. In equinox (winter) when the sunrise terminator is orientated meridionally (more eastward), the westward magnetic declination at MH causes later sunrise in the E-region than F-region on the same field line, which helps sustain PEFs. Furthermore, the observed TID wavefronts with a meridional alignment in the early morning seems necessary to maintain the PEFs, as extensively discussed previously (Tsunoda, 2010; Krall et al., 2013; Chou et al., 2018; Varney et al., 2009).

As waves progressed toward midday with larger ionospheric conductivities, clockwise rotation in TID fronts could occur from meridional elongation to partial zonal orientation. Alternately, GW forcing could dissipate over time. Alone or in combination, these effects would weaken GW-driven PEFs, leaving zonal ion drifts dominated by a background E-region dynamo under quiet conditions (Sq) or influenced by geomagnetic disturbances.

Further evidence of midlatitude PEFs existing within TIDs/GWs is provided by the opposite signs of V_{east} in the topside and bottomside ionosphere (Figure 2d,e). This is consistent with positive and negative charge separation in the topside and bottomside, producing oppositely directed PEFs (Heelis, 2004). Figures 4b,c provide a PEF development scenario in the vertical-meridional direction considering generic electrostatic constrains (divergent-free currents, curl-free electric fields, and equal-potential F-region field lines). An alternative mechanism with GW horizontal and vertical oscillations could be sufficient to account for the observed zonal and vertical ion drifts, however, the GW vertical wavelength should be relatively larger than the vertical thickness of the conductive F layer in order to maintain the PEF; PEFs associated with shorter vertical wavelength GWs may be entirely smeared out. We note that V_{east} pattern is well-established at post-sunset equatorial latitudes (e.g. Kudeki & Bhattacharyya, 1999; Martinis et al., 2003) where, together with vertical drifts, an “evening vortex” can develop. Our observations, represented here by 2018-09-04, are consistent with a dynamic vortex pattern in the zonal-vertical plane during TID zonal propagation.

These results imply that ST-time midlatitude TIDs were not a simple manifestation of GWs, even though TIDs had several signatures imposed by GW properties. Rather, the electrified nature of the TIDs produced zonal propagation in a similar fashion as neutrals in GWs, but with different wave vectors and periods (Hines & Hooke, 1970) and different dynamic features. Although excited differently, the observed electrified waves possess some similarities to reported nighttime MSTIDs at midlatitudes (Makela & Otsuka, 2011; Otsuka et al., 2004), and electric fields embedded in those nighttime TIDs were also identified previously (Saito et al., 1995; Shiokawa et al., 2003).

Finally, it is useful to consider the possible conjugate appearance of these electrified TIDs, since the associated PEFs could potentially be mapped into the conjugate hemisphere along the magnetic field. Figure 3f provides coarse (due to sparse data coverage)

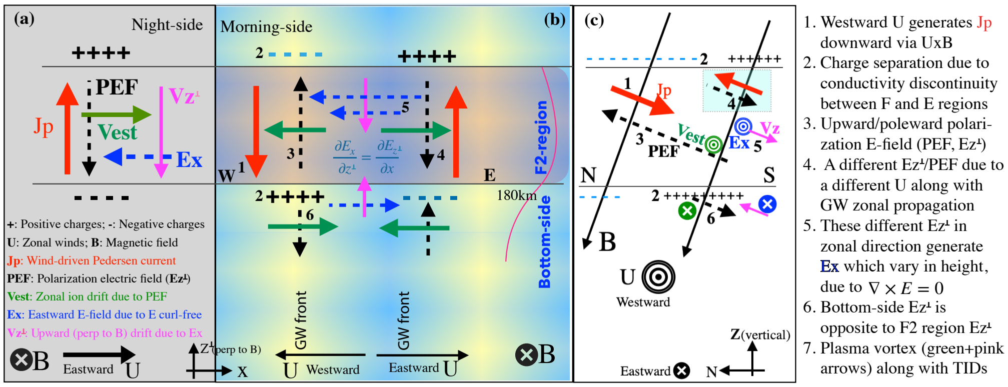

Figure 4. One scenario of GW zonal wind-induced electrodynamics. Pre-sunrise (a); Post-sunrise (b) in X-Z$^{\perp}$ plane with X eastward and Z$^{\perp}$ upward/northward, perpendicular to **B**, and Z (vertical)-northward plane (c). Key steps explained on the far-right side are numbered in b-c). Step 4 in c) is on a parallel plane as in b).

observations of GNSS TID zonal propagation on 2020-01-29 near Palmer, conjugate to MH. When TIDs occurred after sunrise over Palmer, MH was still in darkness, and indeed some pre-sunrise TIDs were present. 5-6 hours later when MH was at sunrise, Palmer was around noontime and showed no significant TIDs. In general, the 2018-09-04 event registered some potential TIDs at Palmer. However, these results are not definitive as to conjugacy of electrified TIDs since local and conjugate sunrises occurred almost simultaneously and because of data sparseness.

5 Summary

Millstone Hill ISR along with GNSS TEC observations were used to determine post-sunrise midlatitude TID characteristics in Nmax, TEC, and Ne altitude profiles, visualizing vertical and horizontal ionospheric disturbances. The first evidence of periodic PEFs associated with post-sunrise midlatitude TID zonal propagation and electrodynamic features were identified. Key findings are:

1. Post-sunrise TIDs were frequently observed at Millstone Hill. They typically propagated eastward at ~140-150 m/s phase speeds and <60 min periods. The density disturbances had downward phase progression and 70 km vertical wavelength, consistent with GW effects. Some portion of TID wavefronts was initially (in the early morning)

parallel to the ST, but the wavefronts rotated post-sunrise in a few hours towards large zonal alignment.

2. Periodic PEFs embedded in TIDs were identified in the morning hours. They developed as TID partial wavefronts tended meridionally elongated during early morning hours when E-region conductivities were still low. Some of these TIDs appeared as multiple vortices spanning the topside and bottomside ionosphere along a vertical-zonal plane.

Observed ST-time electric fields were consistent with GW zonal-wind dynamo effects, producing V_{east} in the direction of zonal winds while avoiding substantial damping of GWs. Observations also indicated that in the topside, V_{east} fluctuations were highly correlated to those in vertical ion drift and in electron density: an upward vertical ion drift corresponded to a westward V_{east}, and vice versa. However, since topside vertical ion drift fluctuations were attributed to disturbances in GW-induced meridional winds driving ions upward and downward along the magnetic field, a competition at midlatitude between meridional electric fields PEF and ambipolar diffusion would imply that the V_{east} and vertical drift relationship is likely indirect. This requires further quantitative study.

Contrary to conventional GW manifestation expectations, this study emphasized the electrodynamics of post-sunrise TIDs, appearing predominantly (and regularly) with distinct zonal propagation. Effects are ultimately produced by the GW dynamo conversion of neutral kinetic energy to plasma electrical energy.

6 Acknowledgements

MH ISR observation, GNSS TEC data processing, and Madrigal database system are provided to the community by MIT under NSF grant AGS-1952737 support. PJE acknowledges support from this grant. SRZ acknowledges MURI grant ONR15-FOA-0011 and NSF grant AGS-2033787. AJC, SRZ and LPG acknowledge ONR Grant N00014-17-1-2186; LPG acknowledges NASA grant 80NSSC19K0834. ISR and TEC data files were originally downloaded from Madrigal, and have been archived here for direct access:

`https://datadryad.org/stash/share/G_0tzP2sepiyNZaE-oiy_YO3OerxjBFh7-aRPSQbabs`

Data for TEC processing is provided from the following organizations: UNAVCO; SOPAC; IGN (France); IGS; CDDIS; NGS; IBGE (Brazil); RAMSAC (Argentina); CORS (Panama); Arecibo Observatory, LISN; Topcon; CHAIN (Canada); CRS (Italy); SONEL; RENAG (New Zealand); GNSS Reference Networks; Finnish Meteorological Institute; and SWEPOS. We thank both reviewers for their constructive comments.

References

Afraimovich, E., Edemskiy, I., Leonovich, A., Leonovich, L., Voeykov, S., & Yasyukevich, Y. V. (2009). Mhd nature of night-time mstids excited by the solar terminator. *Geophysical research letters*, *36*(15).

Afraimovich, E., Edemskiy, I., Voeykov, S., Yasyukevich, Y. V., & Zhivetiev, I. (2010). Travelling wave packets generated by the solar terminator in the upper atmosphere. *Atmospheric and Oceanic Optics*, *23*(1), 21–27.

Beer, T. (1973). Supersonic generation of atmospheric waves. *Nature*, *242*(5392), 34–34.

Beer, T. (1978). On atmospheric wave generation by the terminator. *Planetary and Space Science*, *26*(2), 185–188.

Chen, J., Wang, W., Lei, J., & Dang, T. (2020). The physical mechanisms for the sunrise enhancement of equatorial ionospheric upward vertical drifts. *Journal of Geophysical Research: Space Physics*, *125*(8), e2020JA028161. Retrieved from https://agupubs.onlinelibrary.wiley.com/doi/abs/10.1029/2020JA028161 (e2020JA028161 2020JA028161) doi: https://doi.org/10.1029/2020JA028161

Chimonas, G. (1970). Internal gravity-wave motions induced in the earths atmosphere by a solar eclipse. *Journal of Geophysical Research*, *75*(28), 5545–5551.

Chimonas, G., & Hines, C. O. (1970, February). Atmospheric gravity waves induced by a solar eclipse. *Journal of Geophysical Research: Space Physics (1978–2012)*, *75*(4), 875–875.

Chou, M.-Y., Lin, C. C. H., Shen, M.-H., Yue, J., Huba, J. D., & Chen, C.-H. (2018). Ionospheric disturbances triggered by spacex falcon heavy. *Geophysical Research Letters*, *45*(13), 6334-6342. Retrieved from https://agupubs.onlinelibrary.wiley.com/doi/abs/10.1029/2018GL078088 doi: https://doi.org/10.1029/2018GL078088

Djuth, F., Sulzer, M., Gonzales, S., Mathews, J., Elder, J., & Walterscheid, R. (2004). A continuum of gravity waves in the arecibo thermosphere? *Geophysical Research Letters*, *31*(16).

Eccles, J. V., Maurice, J. P. S., & Schunk, R. W. (2015, June). Mechanisms underlying the prereversal enhancement of the vertical plasma drift in the low-latitude ionosphere. *Journal of Geophysical Research: Space Physics*, *120*(6), 4950–4970.

Eisenbeis, J., Occhipinti, G., Astafyeva, E., & Rolland, L. (2019). Short-and long-wavelength tids generated by the great american eclipse of 21 august 2017. *Journal of Geophysical Research: Space Physics*, *124*(11), 9486–9493.

Evans, J. V. (1968, June). Sunrise behavior of the F layer at midlatitudes. *Journal of Geophysical Research: Space Physics (1978–2012)*, *73*(11), 3489–3504.

Farley, D., Bonelli, E., Fejer, B. G., & Larsen, M. (1986). The prereversal enhancement of the zonal electric field in the equatorial ionosphere. *Journal of Geophysical Research: Space Physics*, *91*(A12), 13723–13728.

Forbes, J. M., Bruinsma, S. L., Miyoshi, Y., & Fujiwara, H. (2008). A solar terminator wave in thermosphere neutral densities measured by the champ satellite. *Geophysical Research Letters*, *35*(14).

Galushko, V., Paznukhov, V., Yampolski, Y., & Foster, J. (1998). Incoherent scatter radar observations of agw/tid events generated by the moving solar terminator. *Annales Geophysicae*, *16*(7), 821–827.

Haerendel, G., & Eccles, J. V. (1992, February). The role of the equatorial electrojet in the evening ionosphere. *Journal of Geophysical Research: Space Physics (1978–2012)*, *97*(A2), 1181–1192.

Hedlin, M., de Groot-Hedlin, C., Forbes, J., & Drob, D. (2018). Solar terminator waves in surface pressure observations. *Geophysical Research Letters*, *45*(10), 5213–5219.

Heelis, R. A. (2004, July). Electrodynamics in the low and middle latitude ionosphere: A tutorial. *Journal of Atmospheric and Solar-Terrestrial Physics*, *66*(10), 825–838.

Heelis, R. A., Crowley, G., Rodrigues, F., Reynolds, A., Wilder, R., Azeem, I., & Maute, A. (2012, August). The role of zonal winds in the production of a prereversal enhancement in the vertical ion drift in the low latitude ionosphere.

Journal of Geophysical Research: Space Physics (1978–2012), *117*(A8).

Hines, C., & Hooke, W. (1970). Discussion of ionization effects on the propagation of acoustic-gravity waves in the ionosphere. *Journal of Geophysical Research*, *75*(13), 2563–2568.

Huba, J., Drob, D., Wu, T.-W., & Makela, J. J. (2015). Modeling the ionospheric impact of tsunami-driven gravity waves with sami3: Conjugate effects. *Geophysical Research Letters*, *42*(14), 5719–5726.

Huba, J., Joyce, G., & Fedder, J. (2000). Ion sound waves in the topside low latitude ionosphere. *Geophysical research letters*, *27*(19), 3181–3184.

Hysell, D., Larsen, M., Fritts, D., Laughman, B., & Sulzer, M. (2018). Major upwelling and overturning in the mid-latitude f region ionosphere. *Nature communications*, *9*(1), 1–11.

Kelley, M. C., Rodrigues, F. S., Pfaff, R. F., & Klenzing, J. (2014, September). Observations of the generation of eastward equatorial electric fields near dawn. *Annales Geophysicae*, *32*(9), 1169–1175.

Kirchengast, G., Hocke, K., & Schlegel, K. (1996, January). The gravity wave-TID relationship: insight via theoretical model—EISCAT data comparison. *Journal of atmospheric and terrestrial physics*, *58*(1-4), 233–243.

Krall, J., Huba, J. D., Joyce, G., & Hei, M. (2013). Simulation of the seeding of equatorial spread f by circular gravity waves. *Geophysical Research Letters*, *40*(1), 1-5. Retrieved from `https://agupubs.onlinelibrary.wiley.com/doi/abs/10.1029/2012GL054022` doi: https://doi.org/10.1029/2012GL054022

Kudeki, E., & Bhattacharyya, S. (1999). Postsunset vortex in equatorial f-region plasma drifts and implications for bottomside spread-f. *Journal of Geophysical Research: Space Physics*, *104*(A12), 28163–28170.

Liu, C. H., & Yeh, K. C. (1969, May). Effect of ion drag on propagation of acoustic-gravity waves in the atmospheric F region. *Journal of Geophysical Research: Space Physics (1978–2012)*, *74*(9), 2248–2255.

Liu, H., Lühr, H., & Watanabe, S. (2009). A solar terminator wave in thermospheric wind and density simultaneously observed by champ. *Geophysical Research Letters*, *36*(10).

Liu, J. Y., Sun, Y. Y., Kakinami, Y., Chen, C. H., Lin, C. H., & Tsai, H. F. (2011).

Bow and stern waves triggered by the moon's shadow boat. *Geophysical Research Letters*, *38*(17). Retrieved from https://agupubs.onlinelibrary.wiley.com/doi/abs/10.1029/2011GL048805 doi: https://doi.org/10.1029/2011GL048805

Makela, J. J., & Otsuka, Y. (2011, August). Overview of Nighttime Ionospheric Instabilities at Low- and Mid-Latitudes: Coupling Aspects Resulting in Structuring at the Mesoscale. *Space Science Reviews*, *168*(1-4), 419–440.

Mallat, S. (1999). *A wavelet tour of signal processing.* Elsevier.

Martinis, C., Eccles, J. V., Baumgardner, J., Manzano, J., & Mendillo, M. (2003, January). Latitude dependence of zonal plasma drifts obtained from dual-site airglow observations. *Journal of Geophysical Research: Space Physics*, *108*(A3), 1129.

Medvedev, A. S., Yiit, E., & Hartogh, P. (2017). Ion friction and quantification of the geomagnetic influence on gravity wave propagation and dissipation in the thermosphere-ionosphere. *Journal of Geophysical Research: Space Physics*, *122*(12), 12,464-12,475. Retrieved from https://agupubs.onlinelibrary.wiley.com/doi/abs/10.1002/2017JA024785 doi: https://doi.org/10.1002/2017JA024785

Miyoshi, Y., Fujiwara, H., Forbes, J. M., & Bruinsma, S. L. (2009). Solar terminator wave and its relation to the atmospheric tide. *Journal of Geophysical Research: Space Physics*, *114*(A7).

Nygrn, T., Aikio, A. T., Voiculescu, M., & Cai, L. (2015). Radar observations of simultaneous traveling ionospheric disturbances and atmospheric gravity waves. *Journal of Geophysical Research: Space Physics*, *120*(5), 3949-3960. Retrieved from https://agupubs.onlinelibrary.wiley.com/doi/abs/10.1002/2014JA020794 doi: https://doi.org/10.1002/2014JA020794

Otsuka, Y., Shiokawa, K., Ogawa, T., & Wilkinson, P. (2004). Geomagnetic conjugate observations of medium-scale traveling ionospheric disturbances at midlatitude using all-sky airglow imagers. *Geophysical research letters*, *31*(15).

Panasenko, S. V., Goncharenko, L. P., Erickson, P. J., Aksonova, K. D., & Domnin, I. F. (2018). Traveling ionospheric disturbances observed by kharkiv and millstone hill incoherent scatter radars near vernal equinox and summer solstice. *Journal of Atmospheric and Solar-Terrestrial Physics*, *172*, 10–23.

Rishbeth, H. (1971, February). The F-layer dynamo. *Planetary and Space Science*, *19*(2), 263–267.

Rishbeth, H., Jenkins, B., & Moffett, R. (1995). The f-layer at sunrise. In *Annales geophysicae* (Vol. 13, pp. 367–374).

Rishbeth, H., & Setty, C. (1961). The f-layer at sunrise. *Journal of Atmospheric and Terrestrial Physics*, *20*(4), 263–276.

Saito, A., Iyemori, T., Sugiura, M., Maynard, N. C., Aggson, T. L., Brace, L. H., ... Yamamoto, M. (1995, November). Conjugate occurrence of the electric field fluctuations in the nighttime midlatitude ionosphere. *Journal of Geophysical Research: Space Physics (1978–2012)*, *100*(A11), 21439–21451.

Savitzky, A., & Golay, M. J. E. (1964). Smoothing and differentiation of data by simplified least squares procedures. *Analytical Chemistry*, *36*, 1627-1639.

Shiokawa, K., Otsuka, Y., Ihara, C., Ogawa, T., & Rich, F. (2003). Ground and satellite observations of nighttime medium-scale traveling ionospheric disturbance at midlatitude. *Journal of Geophysical Research: Space Physics*, *108*(A4).

Somsikov, V. (2011). Solar terminator and dynamic phenomena in the atmosphere: A review. *Geomagnetism and Aeronomy*, *51*(6), 707–719.

Somsikov, V., & Trotskii, B. (1975). Generation of disturbances in the atmosphere during the passage of the solar terminator through it. *Geomagn. Aeron.(USSR)(Engl. Transl.);(United States)*, *15*(5).

Song, Q., Ding, F., Wan, W., Ning, B., Liu, L., Zhao, B., ... Zhang, R. (2013). Statistical study of large-scale traveling ionospheric disturbances generated by the solar terminator over china. *Journal of Geophysical Research: Space Physics*, *118*(7), 4583–4593.

Tsunoda, R. T. (2010). On seeding equatorial spread f: Circular gravity waves. *Geophysical Research Letters*, *37*(10). Retrieved from `https://agupubs.onlinelibrary.wiley.com/doi/abs/10.1029/2010GL043422` doi: https://doi.org/10.1029/2010GL043422

Vadas, S. L. (2007, June). Horizontal and vertical propagation and dissipation of gravity waves in the thermosphere from lower atmospheric and thermospheric sources. *Journal of Geophysical Research: Space Physics (1978–2012)*, *112*(A6).

Varney, R. H., Kelley, M. C., & Kudeki, E. (2009). Observations of electric fields associated with internal gravity waves. *Journal of Geophysical Research: Space Physics*, *114*(A2). Retrieved from `https://agupubs.onlinelibrary.wiley.com/doi/abs/10.1029/2008JA013733` doi: https://doi.org/10.1029/2008JA013733

Vasylyev, V., & Sergeev, V. (1999). Speed-resonant terminator wave generation in the earth troposphere. *Earth, Moon, and Planets*, *84*(2), 81–93.

Vierinen, J., Bhatt, A., Hirsch, M. A., Strømme, A., Semeter, J. L., Zhang, S.-R., & Erickson, P. J. (2016, January). High temporal resolution observations of auroral electron density using superthermal electron enhancement of Langmuir waves. *Geophyical Research Letters*.

Zhang, R., Liu, L., Chen, Y., & Le, H. (2015). The dawn enhancement of the equatorial ionospheric vertical plasma drift. *Journal of Geophysical Research: Space Physics*, *120*(12), 10,688-10,697. Retrieved from `https://agupubs.onlinelibrary.wiley.com/doi/abs/10.1002/2015JA021972` doi: https://doi.org/10.1002/2015JA021972

Zhang, S.-R., Coster, A. J., Erickson, P. J., Goncharenko, L. P., Rideout, W., & Vierinen, J. (2019, July). Traveling Ionospheric Disturbances and Ionospheric Perturbations Associated With Solar Flares in September 2017. *Journal of Geophysical Research: Space Physics*, *60*(8), 895.

Zhang, S.-R., Erickson, P. J., Goncharenko, L. P., Coster, A. J., Rideout, W., & Vierinen, J. (2017, December). Ionospheric Bow Waves and Perturbations Induced by the 21 August 2017 Solar Eclipse. *Geophyical Research Letters*, *44*(2), 12–.

Zhang, S.-R., Erickson, P. J., Zhang, Y., Wang, W., Huang, C., Coster, A. J., ... Kerr, R. (2017, January). Observations of ion-neutral coupling associated with strong electrodynamic disturbances during the 2015 St. Patrick's Day storm. *Journal of Geophysical Research: Space Physics*, *122*(1), 1314–1337.

Zhu, L., Schunk, R. W., Eccles, V., Scherliess, L., Sojka, J. J., & Gardner, L. (2017, November). Terminator field-aligned current system: Its dependencies on solar, seasonal, and geomagnetic conditions. *Journal of Atmospheric and Solar-Terrestrial Physics*, *164*, 10–17.